applied optics

Substrate aberration and correction for meta-lens imaging: an analytical approach

Benedikt Groever,[1] Charles Roques-Carmes,[1,2] Steven J. Byrnes,[3] and Federico Capasso[1,*]

[1]*Harvard John A. Paulson School of Engineering and Applied Sciences, Harvard University, Cambridge, Massachusetts 02138, USA*
[2]*Research Laboratory of Electronics, Massachusetts Institute of Technology, Cambridge, Massachusetts 02139, USA*
[3]*Charles Stark Draper Laboratory, Cambridge, Massachusetts 02139, USA*
*Corresponding author: capasso@seas.harvard.edu

Meta-lenses based on flat optics enabled a fundamental shift in lens production—providing an easier manufacturing process with an increase in lens profile precision and a reduction in size and weight. Here we present an analytical approach to correct spherical aberrations caused by light propagation through the substrate by adding a substrate-corrected phase profile, which differs from the original hyperbolic one. A meta-lens encoding the new phase profile would yield diffraction-limited focusing and an increase of up to 0.3 of its numerical aperture without changing the radius or focal length. In tightly focused laser spot applications such as direct laser lithography and laser printing, a substrate-corrected meta-lens can reduce the spatial footprint of the meta-lens. © 2018 Optical Society of America

OCIS codes: (050.1965) Diffractive lenses; (050.5080) Phase shift; (050.6624) Subwavelength structures.

https://doi.org/10.1364/AO.57.002973

1. INTRODUCTION

In recent years, metasurfaces have emerged as a new way to control light through the optical properties of sub-wavelength elements patterned on the flat surface of a substrate. A sub-wavelength element can locally change the amplitude, polarization, and phase of an incident electromagnetic wave to realize various optical functions in a compact configuration [1–6]. A metasurface can be produced through a single lithography step of nanofabrication, which can be scaled easily to high-output manufacturing processes.

One of the most promising applications of metasurfaces is imaging. Here, each sub-wavelength element corresponds to one data point of the discretized phase profile of the meta-lens. Due to sub-wavelength spacing, light sees a near-continuous phase profile. During fabrication, the dimensions of the sub-wavelength elements are well controlled, enabling high lens profile precision. A diffraction-limited focal spot can be achieved [7]. The lens profile precision of conventional refractive lenses depends on the accuracy of the lens curvature, which is more difficult to control [8]. Future challenges of meta-lenses lay in the correction of chromatic aberrations, which can be reduced by several approaches such as by using refractive/diffractive compound lenses [9], dispersion engineering of nanostructure resonances [10,11], or designing a nanostructure that has control over group velocity delay and has the capability of a 2π phase modulation [12–14]. This would allow circumventing the current limitations encountered in diffractive optics [15–17].

To fabricate a working meta-lens, a substrate is essential for arranging the sub-wavelength elements. However, any transparent glass substrate has a refractive front surface. As of now, the refractive front surface has not played a major role in the development of meta-lenses, because most meta-lenses were designed to focus a normal incident beam [7,18,19]. However, in the general point-to-point imaging configuration with finite object and imaging distances, incidence is no longer normal. Refraction occurs at the front surface of the substrate—where the front surface of the substrate is the surface with no meta-lens—causing spherical aberrations. In this paper, we introduce an analytical phase profile, which corrects the spherical aberrations caused by the front surface of the substrate. Our approach also offers physical insight on how Seidel aberrations respond to changes in meta-lens design. Previously such substrate corrections were only performed with ray-tracing techniques [20]. Without correction of those aberrations, it is in general not possible to achieve diffraction-limited focusing at high numerical apertures (NAs) in point-to-point imaging systems.

Besides overcoming spherical aberrations, there are also other advantages. The substrate-corrected phase profile allows mounting the meta-lens on the substrate side opposing the focal spot, thus protecting the meta-lens better from contaminants in the outside world, such as dust and humidity; this is important for applications in microscopy [21,22] where the lens is close to the specimen. We also find that this configuration has a higher NA and therefore a smaller

diffraction-limited focal spot. This would be useful for focusing applications that require a tightly focused laser spot, such as direct laser lithography and laser printing [23].

Aberration correction plays a major role in the development of high-resolution imaging systems for machine vision, computer vision, and microscopy applications. A single, planar lens cannot produce a diffraction-limited spot along the focal plane mostly due to Petzval field curvature and coma aberration [24,25]. Recently, a diffraction-limited meta-lens doublet along the focal plane in the visible has been demonstrated [26]. For the development of new kinds of meta-lens objectives, ray tracing optimization is needed [26,27]. Our analytical substrate-corrected phase profile can be used to better predict the initial optimization parameters [8,28,29].

2. HYPERBOLIC META-LENS AND SUBSTRATE-CORRECTED META-LENS

Meta-lenses that are designed for focusing a normal incident beam, which remains collimated inside the substrate, are characterized by a hyperbolic phase profile [24]:

$$\varphi(\rho) = -\frac{2\pi}{\lambda_0} n_{\mathrm{m}} \left(\sqrt{\rho^2 + f^2} - f \right). \tag{1}$$

This formula gives the required shift at each radial coordinate to achieve diffraction-limited focusing at a focal length of f. λ_0 is the (free-space) illumination wavelength and n_{m} is the refractive index of the ambient medium ($n_{\mathrm{m}} = 1$). Figure 1(a) shows the ray diagram of a meta-lens with a hyperbolic phase profile mounted on a substrate, referred to as a hyperbolic meta-lens (HML) hereafter. Collimated light is incident from the front surface of the substrate. The meta-lens is mounted on the other side of the substrate. The incident beam remains collimated in the substrate. The HML performs diffracted-limited focusing. We refer to diffraction-limited focusing when all rays for a given angle of incidence intersect the optical axis at the same position. Amplitude variations of the incoming electric field caused by absorption or reflection only need to be considered once the system is diffraction-limited, as they influence the shape of the focal spot, e.g., removal of the Airy disk caused by diffraction, which is known as apodization. Ray tracing is sufficient to achieve diffraction-limited focusing. Figure 1(b) shows the performance of a HML when collimated light is incident from the meta-lens side. Here refraction in the substrate leads to a spherically aberrated focal spot. In this paper, we present an analytical approach to design a meta-lens to compensate for the refractive properties of the substrate, so that when light is incident from the meta-lens side, it enables diffraction-limited focusing as shown in Fig. 1(d). The meta-lens with a substrate-corrected phase profile, referred to as a substrate-corrected meta-lens (SCML) hereafter, has a larger phase gradient than a HML of the same focal length [Fig. 1(c)]. The larger phase gradient at the edge of the SCML corrects for light propagation through the substrate. Conversely, since the SCML is designed for light to be collimated on the meta-lens side, and if it is illuminated with collimated light from the substrate side, it results in a spherically aberrated focal spot as shown in Fig. 1(e). The fact that the HML and SCML are diffraction-limited only for one direction of incidence is not
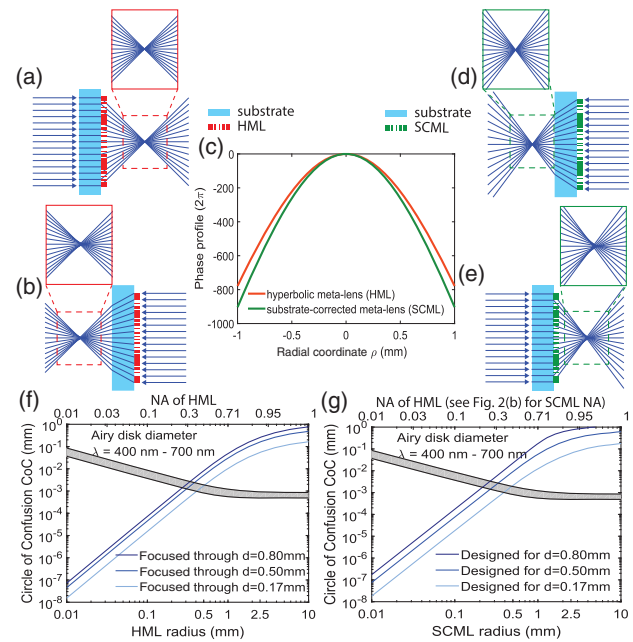

Fig. 1. Focusing of a HML and a SCML with incident collimated light from different sides of the substrate. (a) Ray diagram for diffraction-limited focusing with the HML. Light is incident from the front surface of the substrate and every ray intersects the optical axis at the designed focal length. (b) Ray diagram for aberrated focusing with the HML. In this configuration, where light is incident from the backside of the substrate, spherical aberration exists due to refraction at the front surface of the substrate. (c) Phase profiles of the SCML and HML [Eqs. (6) and (7), respectively]. (d) Ray diagram for diffraction-limited focusing with the SCML. Light is incident from the meta-lens side. The steeper phase profile of the SCML takes the refraction at the front surface of the substrate into account, in such a way that every ray intersects with the optical axis at the same position. (e) Ray diagram for aberrated focusing with the SCML. Panels (f) and (g) show CoC as a function of HML–SCML meta-lens radius, for light focused through different substrate thicknesses d. For all meta-lenses depicted, $f = 1.0$ mm, $n_{\mathrm{sub}} = 1.46$, and $n_{\mathrm{m}} = 1$. For the meta-lenses in (a)–(e), substrate thickness $d = 0.50$ mm. For the meta-lenses in (c), illumination wavelength $\lambda_0 = 532$ nm; the results in the other subfigures are independent of the illumination wavelength as the $1/k_0$ factor in the generalized Snell's law cancels the illumination wavelength.

specific to meta-lenses. Refractory plano-convex aspherical lenses, which are used to focus collimated light, have the same kind of directional behavior. In what follows, we will refer to a configuration for a meta-lens as a "wrong" configuration when it is illuminated in such a way as to produce a spherically aberrated focal spot, and "right" configuration when illumination results in a diffraction-limited spot.

The minimum achievable focal spot size for a meta-lens used in the wrong configuration is shown in Figs. 1(f) and 1(g), respectively, for the HML and SCML. The figure of merit is the Circle of Confusion (CoC). The circle containing all incident rays is an important figure of merit for the size of the focal spot. The CoC is defined as the minimum circle, when moving along the optical axis. Images are sharpest when the image detector is at this position. As each meta-lens is only diffraction-limited for

normal incidence in the right configuration, we consider only normal incidence in the wrong configuration. A rule of thumb to characterize a diffraction-limited system is to verify that all rays fall within a disk of diameter $d_{Airy} = 1.22(\lambda_0/NA)$, where NA is the NA. d_{Airy} is roughly the diameter of the diffraction-limited Airy disk; when this criterion is satisfied, the point-spread function should be only modestly different from the ideal Airy pattern. The diffraction-limited Airy disk as a function of radius for the HML and SCML is shown as a shaded area in Figs. 1(f) and 1(g), respectively. Figure 1(f) shows that a HML with a focal length of 1 mm used in the wrong configuration can still create a diffraction-limited spot if the NA is smaller than 0.3. Conversely, Fig. 1(g) shows that a SCML with a focal length of 1 mm used in the wrong configuration (i.e., collimated on the substrate side) can be diffraction-limited up to a radius of 0.25 mm, corresponding to a NA of 0.3–0.4, depending on the thickness of the substrate [Fig. 2(b)].

The size of the Airy disk depends only on the NA of an imaging system—not on the actual focal length or radius. When scaling the focal length and radius of the lens, the CoC scales with the same factor, but the size of the Airy disk does not change. Therefore, it is harder to achieve diffraction-limited focusing with a lens when the radius of the lens increases.

3. PHASE PROFILE OF A DIFFRACTION-LIMITED POINT-TO-POINT FOCUSING META-LENS

Now we discuss the point-to-point imaging configuration. The above discussion (∞ to f or f to ∞) is a particular case in which one point is at infinity. In a point-to-point imaging configuration, we need to consider an object point source located in front of the meta-lens, which gets focused to an image point on the other side of the meta-lens. We call the distance from the object point source to the meta-lens the "designed front distance," d_f, and the distance from the meta-lens to the image
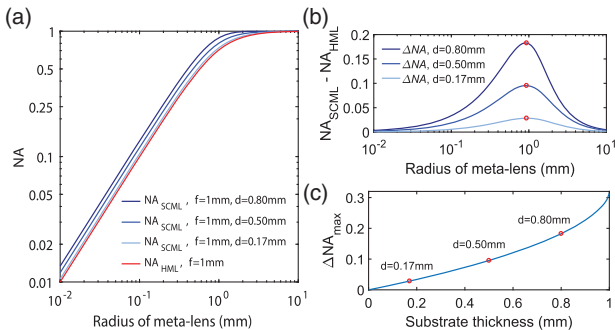

Fig. 2. NA of a SCML in comparison with that of a HML. (a) NA of a HML for different radii and NA of a SCML for different radii and substrate thicknesses d. In the limit of a small substrate thickness, the NA of the SCML approaches the NA of the HML. (b) NA difference (ΔNA), $NA_{SCML} - NA_{HML}$, for different radii and substrate thicknesses d. The maximum of ΔNA occurs for all SCMLs at a radius of 932.6 μm. (c) Maximum of ΔNA for different substrate thicknesses d. The points that are equivalent in subfigures (b) and (c) are marked with red circles. For all meta-lenses depicted, $f = 1$ mm, $n_{sub} = 1.46$, and $n_m = 1$.
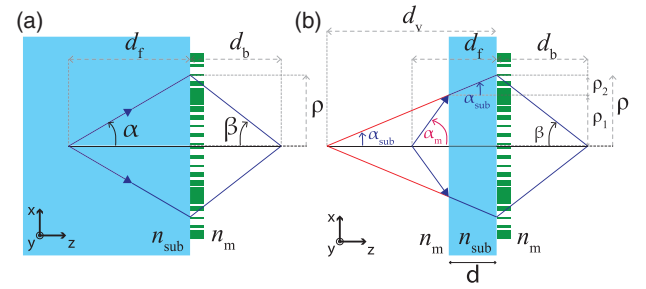

Fig. 3. Point-to-point metasurface focusing. (a) Ray diagram of a meta-lens (dark green rectangles) mounted on an infinitely extended substrate. The image (focal spot) is inside the substrate and the object point is in the ambient medium, both on the optical axis. The designed front distance and the designed back distance are denoted with d_f and d_b, respectively. (b) Ray diagram of a meta-lens mounted on a substrate of a finite thickness d, and the object and image spots are in the ambient medium. Light from a point source along the optical axis at a distance of d_f from the meta-lens is focused to a point at distance of d_b from the meta-lens. The distance from the intersection of the virtual rays (red lines) with the optical axis to the meta-lens is defined as the virtual front distance d_v. The virtual front distance $d_v(\rho)$ is a function of the radial coordinate ρ.

point the "designed back distance," d_b (Fig. 3). The lens will work best (i.e., at the diffraction limit) when focusing light from the designed front point to the designed back point or vice versa. In what follows, we shall assume that the lens is operating in this way, with the object point source at the designed front position and the image point at the designed back position. The object point source will still generally be focused if it is somewhere else on the optical axis, although the image point will have spherical aberrations. These spherical aberrations are not related to the substrate, but rather are inevitable due to the fixed phase profile of the optical system. Their correction would require a variable imaging system, e.g., with varifocal meta-lenses [30], which can be tuned to track the object's position. Such systems are widely used in cameras. To derive the phase profile of a meta-lens for diffraction-limited point-to-point focusing, we shall first consider the case of a meta-lens mounted on an infinite extended substrate, $-\infty < z < 0$, as shown in Fig. 3(a). The object point source and designed front distance are inside the substrate with a refractive index of n_{sub}. The image point and designed back distance are in the ambient medium. We assume that the generalized Snell's law applies at the interface [1]:

$$\frac{1}{k_0}\frac{d\varphi}{d\rho} = n_m \sin\beta - n_{sub} \sin\alpha. \quad (2)$$

Here $k_0 = 2\pi/\lambda_0$. α and β are expressed as $\alpha = \arctan(\rho/d_f)$ and $\beta = \arctan(-\rho/d_b)$, respectively, and $\rho = \sqrt{x^2 + y^2}$ has x and y as the position coordinates on the meta-lens while the optical axis is at $x = y = 0$ along z direction. The generalized Snell's law is valid once the height of the dielectric meta-lens is sufficiently sub-wavelength, the transmission is near unity, and the separation is sub-wavelength. With the identity $\sin(\arctan(x)) = x/(1 + x^2)^{1/2}$, Eq. (2) can be written as

$$\frac{1}{k_0}\frac{d\varphi}{d\rho} = -n_{\mathrm{m}}\frac{\rho}{\sqrt{d_{\mathrm{b}}^2 + \rho^2}} - n_{\mathrm{sub}}\frac{\rho}{\sqrt{d_{\mathrm{f}}^2 + \rho^2}}.$$

Integration of the above equation leads to

$$\varphi(\rho) = -k_0 n_{\mathrm{m}}\sqrt{d_{\mathrm{b}}^2 + \rho^2} - k_0 n_{\mathrm{sub}}\sqrt{d_{\mathrm{f}}^2 + \rho^2}. \qquad \textbf{(3)}$$

This is the required phase profile for diffraction-limited point-to-point focusing of a meta-lens mounted on an infinite extended substrate. In the next step, we assume a substrate of thickness d and $d < d_{\mathrm{f}}$. We virtually extend to the optical axis [red line in Fig. 3(b)] the rays refracted into the substrate. The distance between the intersection of the virtual rays with the optical axis and the meta-lens is the virtual front distance d_{v}. The angle in the substrate, α_{sub}, of the ray is given by

$$\sin\alpha_{\mathrm{sub}} = \frac{\rho}{\sqrt{d_{\mathrm{v}}^2 + \rho^2}}.$$

Using Snell's law, $\sin\alpha_{\mathrm{sub}} = \sin\alpha_{\mathrm{m}}n_{\mathrm{m}}/n_{\mathrm{sub}}$, at the front surface of the substrate yields

$$\frac{n_{\mathrm{m}}}{n_{\mathrm{sub}}}\sin\alpha_{\mathrm{m}} = \frac{\rho}{\sqrt{d_{\mathrm{v}}^2 + \rho^2}}.$$

Rewriting $\sin\alpha_{\mathrm{m}}$,

$$\frac{n_{\mathrm{m}}}{n_{\mathrm{sub}}}\frac{\rho_1}{\sqrt{(d_{\mathrm{f}} - d)^2 + \rho_1^2}} = \frac{\rho}{\sqrt{d_{\mathrm{v}}^2 + \rho^2}}.$$

ρ_1 is an auxiliary variable with no physical meaning—used to simplify the math. Important is the radial coordinate ρ, which is given by $\rho = \rho_1 + \rho_2$. ρ_1 can be rewritten using similar triangles as $\rho_1 = \rho(d_{\mathrm{v}} - d)/d_{\mathrm{v}}$. Using this identity allows rewriting the previous equation as follows:

$$\frac{n_{\mathrm{m}}}{n_{\mathrm{sub}}}\frac{\rho}{d_{\mathrm{v}}}\frac{(d_{\mathrm{v}} - d)}{\sqrt{(d_{\mathrm{f}} - d)^2 + \frac{\rho^2}{d_{\mathrm{v}}^2}(d_{\mathrm{v}} - d)^2}} = \frac{\rho}{\sqrt{d_{\mathrm{v}}^2 + \rho^2}}.$$

It can be rewritten as a fourth-order polynomial as follows:

$$d_{\mathrm{v}}^4 + a_3 d_{\mathrm{v}}^3 + a_2 d_{\mathrm{v}}^2 + a_1 d_{\mathrm{v}} + a_0 = 0, \qquad \textbf{(4)}$$

where

$$a_3 = (-2d),$$

$$a_2 = (d^2 + \rho^2) - \left(\frac{n_{\mathrm{sub}}}{n_{\mathrm{m}}}\right)^2(\rho^2 + (d_{\mathrm{f}} - d)^2),$$

$$a_1 = \left[1 - \left(\frac{n_{\mathrm{sub}}}{n_{\mathrm{m}}}\right)^2\right](-2d\rho^2),$$

$$a_0 = \left[1 - \left(\frac{n_{\mathrm{sub}}}{n_{\mathrm{m}}}\right)^2\right](d^2\rho^2).$$

Equation (4) can only be solved analytically with great complication as it cannot be reduced to a lower order. The analytical solution is shown in Code 1, Ref. [31]. The phase gradient for diffraction-limited point-to-point focusing with a finite-substrate meta-lens can be obtained by replacing the designed front distance in Eq. (2) with the virtual front distance:

$$\frac{1}{k_0}\frac{d\varphi}{d\rho} = -n_{\mathrm{m}}\frac{\rho}{\sqrt{d_{\mathrm{b}}^2 + \rho^2}} - n_{\mathrm{sub}}\frac{\rho}{\sqrt{d_{\mathrm{v}}(\rho, d_{\mathrm{f}}, d, n_{\mathrm{m}}, n_{\mathrm{sub}})^2 + \rho^2}}.$$

Integration of the above equation gives

$$\varphi(\rho) = -k_0 n_{\mathrm{m}}\sqrt{d_{\mathrm{b}}^2 + \rho^2}$$
$$- k_0 n_{\mathrm{sub}}\int_0^\rho \frac{\rho'}{\sqrt{d_{\mathrm{v}}(\rho', d_{\mathrm{f}}, d, n_{\mathrm{m}}, n_{\mathrm{sub}})^2 + \rho'^2}}d\rho'. \quad \textbf{(5)}$$

The first term of this equation is the phase profile of a HML with a focal distance of d_{b}, whereas the second term is the phase profile of a SCML with a focal distance of d_{f}. A meta-lens with a phase profile as in Eq. (5) yields diffraction-limited point-to-point focusing. This is analogous to combining two aspherical lenses to a biconvex lens in refractive optics.

4. NUMERICAL APERTURES OF A HML AND A SCML

Consider now the phase profiles of two meta-lenses, a HML and a SCML, each with a focal length of f, which is the distance between the focal point and the plane of the meta-lens. Then the phase profiles are given, respectively, by

$$\varphi_{\mathrm{HML}}(\rho) = -k_0 n_{\mathrm{m}}\sqrt{f^2 + \rho^2}, \qquad \textbf{(6)}$$

$$\varphi_{\mathrm{SCML}}(\rho) = -k_0 n_{\mathrm{sub}}\int_0^\rho \frac{\rho'}{\sqrt{f_{\mathrm{v}}(\rho', f, d, n_{\mathrm{m}}, n_{\mathrm{sub}})^2 + \rho'^2}}d\rho'.$$
$$\textbf{(7)}$$

Here $f_{\mathrm{v}}(\rho', f, d, n_{\mathrm{m}}, n_{\mathrm{sub}})$ is the virtual focal length defined as the virtual front distance d_{v} by Eq. (4): $d_{\mathrm{v}} = f_{\mathrm{v}}$. The definition of focal length f should not be mistaken with the front focal length (FFL), back focal length (BFL), or effective focal length (EFL), which are different definitions of a focal length. We choose f as the focal length because it corresponds to the best figure of merit for the spatial footprint of the whole system. The NAs of the SCML and HML are given, respectively, by

$$\mathrm{NA}_{\mathrm{HML}} = n_{\mathrm{m}}\sin\beta = n_{\mathrm{m}}\sin[\arctan(r/f)], \qquad \textbf{(8)}$$

$$\mathrm{NA}_{\mathrm{SCML}} = n_{\mathrm{m}}\sin\alpha = n_{\mathrm{sub}}\sin\alpha_{\mathrm{sub}}$$
$$= n_{\mathrm{sub}}\sin[\arctan(r/f_{\mathrm{v}}(r))], \qquad \textbf{(9)}$$

where NA is, as usual, equal to $\sin\beta$, with β the half-angle of the cone of rays converging to the image point. Here $f_{\mathrm{v}}(r) = f_{\mathrm{v}}(r, f, d, n_{\mathrm{m}}, n_{\mathrm{sub}})$, where r is the radius of the meta-lens. The NA of the SCML depends on not only the radius and focal length of the lens, but also the thickness and refractive index of the substrate. In the limit that the thickness of the substrate, d, approaches 0 or that the ratio of refractive indices $(n_{\mathrm{sub}}/n_{\mathrm{m}})$ approaches unity, the NA of the SCML approaches that of the HML.

Figure 2(a) shows the NAs of the SCML and HML each with a glass substrate ($n_{\mathrm{sub}} = 1.46$) for different radii. As neither the SCML nor the HML is immersed in a high-index liquid, the NA cannot exceed a value greater than unity. The NAs of all meta-lenses increase continuously to maximum values with increase of radius. A SCML has a larger NA than a HML of the same radius and focal length. Similarly, a SCML with a thicker substrate has a NA closer to unity than a SCML with a thinner substrate. Figure 2(b) shows how much larger

the NA of a SCML with different substrate thicknesses is compared with that of a HML, the only limit to increasing substrate thickness being the focal length ($d < f$) of the lens, to remain in a geometry corresponding to Fig. 3(b). At large and small radii, the differences in the value of the NA between the different lenses reach 0. The maximum difference between the SCML and HML for a focal length of 1 mm is reached at a radius of 932.6 μm. We verified that this is true for all substrate thicknesses up to $d = f$. The maximum difference is larger for larger substrate thicknesses as shown in Fig. 2(c). The increase of NA from a HML to a SCML can be as large as 0.3, a limit set by a focal length equal to the thickness of the substrate. This enables a smaller focal spot in a more compact configuration.

5. MAXIMUM ANGLE OF INCIDENCE OF HML AND SCML

Next, we consider off-axis illumination. Here, total internal reflection (TIR) fundamentally limits the functionality of the lens, as beyond a certain angle, light gets reflected instead of being focused. The maximum angle of incidence without TIR, θ_{max} (referred to as maximum angle of incidence hereafter), is an important figure of merit as it limits the field of view and the transmission efficiency of a meta-lens. At the critical angle of TIR, light travels along the surface of the meta-lens as shown in Fig. 4(a) [32,33]. To calculate the critical angle, we begin by applying the generalized Snell's law at the surface of the meta-lens [1]:

$$n_m \sin \theta_m = \frac{1}{k_0} \frac{d\varphi}{d\rho}\bigg]_{\rho=-r} + n_{sub} \sin \theta_{sub}. \qquad (10)$$

We apply it at the lower edge of the meta-lens, which is the radial coordinate ρ with the largest phase gradient. Furthermore, at the critical angle of TIR, the angle in the ambient medium is 90°, $\sin \theta_m = 1$, and the angle in the substrate, θ_{sub}, can be replaced with the maximum angle of incidence by applying Snell's law at the front surface of the substrate: $n_{sub} \sin \theta_{sub} = n_m \sin \theta_m$. The phase gradient at the edge of the HML can be calculated as follows:

$$\frac{1}{k_0} \frac{d\varphi}{d\rho}\bigg]_{\rho=-r} = n_m \frac{r}{\sqrt{f^2 + r^2}} = n_m \sin\left[\arctan\left(\frac{r}{f}\right)\right] = NA.$$

With the above equation and Eq. (10), a criterion for the maximum angle of incidence in terms of the NA of the HML and n_m can be obtained:

$$\sin \theta_{max} = \frac{n_m - NA}{n_m}. \qquad (11)$$

TIR at the lower edge of the HML, $\rho = -r$, corresponds to $\sin \theta_m = 1$ and an angle of incidence of θ_{max}. TIR at the upper edge of the HML, $\rho = r$, corresponds to $\sin \theta_m = -1$ and an angle of incidence of $-\theta_{max}$. In an actual meta-lens, the theoretical value of the maximum angle of incidence, θ_{max}, may not be achieved due to a discretization of the phase profile [1,34], a non-zero thickness, or a non-unity transmission [1]. The HML only has one possible surface for TIR as light at the front surface of the substrate goes from a medium with a lower index (ambient medium) to a medium with a higher index (substrate). For the SCML, we need to consider both surfaces for TIR.
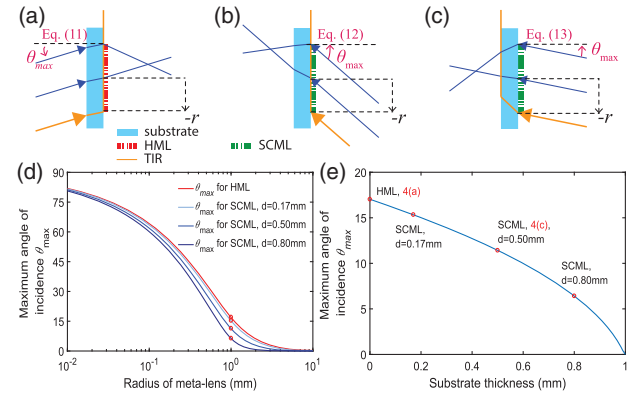

Fig. 4. TIR limitation for maximum angle of incidence of the HML and SCML. When TIR occurs, light propagates along the meta-lenses and consequently limits the maximum angle of incidence. (a) Critical angle of TIR for the marginal ray (orange) at the lower edge of a HML (maximum angle of incidence $\theta_{max} = 17.03°$). When increasing the angle of incidence, the rays closer to the center of the meta-lens would be totally internally reflected further. (b) Critical angle of TIR at the meta-lens surface for the marginal ray at the lower edge of a SCML ($\theta_{max} = 40.15°$). (c) Critical angle of TIR at the front surface of the substrate for the marginal ray at the lower edge of a SCML ($\theta_{max} = 11.42°$). The critical angle of TIR at the front surface of the substrate is always smaller than that at the meta-lens and is, hence, a stricter constraint for the maximum angle of incidence for the SCML. (d) Maximum angle of incidence of the HML and SCML for different radii. The red circles have corresponding data points in subfigure (e)—same radius and substrate thickness. (e) Maximum angle of incidence of the SCML for different substrate thicknesses d. For all meta-lenses depicted, $f = 1$ mm, $n_{sub} = 1.46$, and $n_m = 1$. For the meta-lenses in (a)–(c), $r = 1$ mm and substrate thickness $d = 0.50$ mm. For the meta-lenses in (e), $r = 1$ mm.

As shown in Fig. 4(b), let us first consider the surface with the meta-lens [1]:

$$n_{sub} \sin \theta_{sub} = \frac{1}{k_0} \frac{d\varphi}{d\rho}\bigg]_{\rho=-r} + n_m \sin \theta_{max}.$$

The gradient term in this equation is equal to the NA of the SCML. If this surface has TIR, $\sin \theta_{sub} = \pm 1$, then the criterion for the maximum angle of incidence at the meta-lens surface is given by

$$\sin \theta_{max} = \frac{n_{sub} - NA(r, f, d, n_{sub}, n_m)}{n_m}. \qquad (12)$$

This criterion can be fulfilled only if $\sin \theta_{max} < 1$, and, hence, $NA \geq |n_{sub} - n_m|$; otherwise, the phase gradient at the edge of the meta-lens is too small to exhibit TIR.

Now, let us consider TIR at the refractive front surface of the substrate shown in Fig. 4(c). TIR occurs at this surface when $\sin \theta_m = 1$, and, hence, $\sin \theta_{sub} = n_m/n_{sub}$. Substituting this relation into Eq. (10) eliminates n_{sub}. The following criterion for the maximum angle of incidence can be obtained:

$$\sin \theta_{max} = \frac{n_m - NA(r, f, d, n_{sub}, n_m)}{n_m}. \qquad (13)$$

This constraint for the maximum angle of incidence of an SCML is that of an HML with the same NA. As the refractive

index of the substrate is larger than that of the ambient medium, TIR occurs first at the front surface of the substrate and then at the surface of the SCML; hence, Eq. (13) is a stricter criterion for the maximum angle of incidence than Eq. (12).

Figure 4(d) shows the maximum angle of incidence for a HML and a SCML for different meta-lens radii and substrate thicknesses when the focal length is 1 mm. A SCML with a thicker substrate and a larger radius (and, hence, higher NAs) has a smaller maximum angle of incidence than a HML with equivalent radius and focal length. Figure 4(e) shows the maximum angle of incidence for different substrate thicknesses when the radius and focal length are both 1 mm. As the thickness of the substrate increases, the maximum angle of incidence reduces. This analysis is particularly interesting in the design of a meta-lens stacking that can correct off-axis aberrations.

6. SEIDEL ABERRATIONS OF HML AND SCML

If the HML and SCML are used in the correct configuration, Figs. 1(a) and 1(c), respectively, then spherical aberrations are not present. But besides spherical aberrations, there are four other monochromatic aberrations, namely, distortion, coma aberration, Petzval field curvature, and astigmatism. All five monochromatic aberrations are known as Seidel aberrations. Because of symmetry, astigmatism is not present in a radially symmetric optical system that is infinity-corrected. Therefore, astigmatism is present neither in the HMLs nor in the SCMLs. Coma aberration, Petzval field curvature, and distortion are present in singlet lenses in both conventional refractive lenses and single-layer meta-lenses. For meta-lenses, this is due to the fact that the phase profile to achieve diffraction-limited imaging depends on the angle of incidence. Angle-multiplexed phase profiles that are fully independent can only be implemented through multilayered structures [35] as they provide enough degrees of freedom.

Coma aberration is best known for its resulting comet-shaped image, when observing an off-axis point source. In ray optics, it is defined in terms of the radial coordinate ρ at a given angle of incidence. The magnitude of coma is quantified by the distance between the chief ray and the intersection of two marginal rays, in a plane perpendicular to the optical axis. The two marginal rays have the same angle of incidence as the chief ray and strike the meta-lens plane at coordinates $\pm\rho$ [36] [see Figs. 5(a) and 5(b), and Figs. 5(c) and 5(d) for the HML and SCML, respectively). As the angle of incidence increases, so does the magnitude of coma, and TIR is eventually encountered. We computed the magnitude of coma for different substrates and angles of incidence with a custom-made ray tracing code. The magnitude of coma is smaller for smaller angles of incidence and smaller radial coordinates. As a direct consequence of this observation, meta-lenses with lower NAs exhibit less coma than meta-lenses with larger NAs.

Figure 5(e) shows coma for the HML. We noticed that the HML has the same magnitude of coma as a meta-lens with no substrate. This is true as smaller angles in the substrate of the HML are compensated for by the larger refractive index of the substrate (generalized Snell's law). For the same reason, coma of
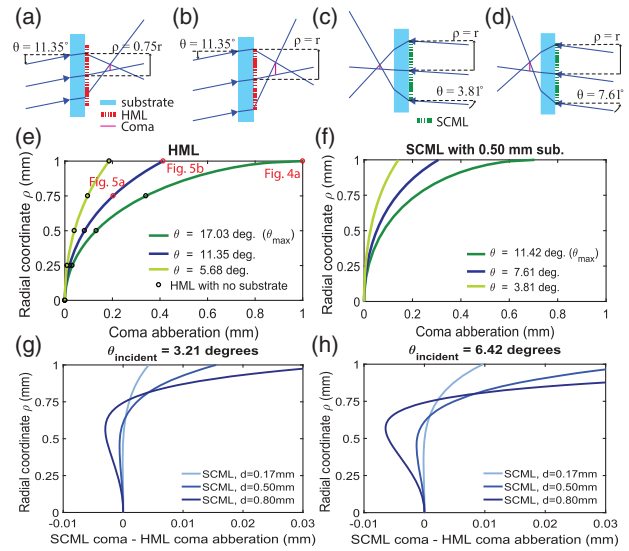

Fig. 5. Coma aberration for a HML and a SCML. Coma is a function of the radial coordinate ρ and angles of incidence θ. (a), (b) Ray diagrams for coma of a HML at an angle of incidence of $\theta = 11.35°$ for radial coordinates of (a) $\rho = 0.75r$ and (b) $\rho = r$. (c), (d) Ray diagrams for coma of the marginal rays at the edge of a SCML for angles of incidence of (c) $\theta = 3.81°$ and (d) $\theta = 7.61°$. The magnitude of coma is smaller for smaller angles of incidence and smaller radial coordinates. (e) Coma of the HML as a function of radial coordinate for different angles of incidence with and without a substrate. The red dots indicate the corresponding ray diagram. The magnitude of coma at the edge of the HML is equal to the radius [Fig. 4(a)]. (f) Coma as a function of radial coordinate for different angles of incidence for the SCML. (g), (h) Coma difference between the SCML and HML for different substrate thicknesses d at angles of incidence of (g) $\theta = 3.21°$ and (h) $\theta = 6.42°$. $\theta = 6.42°$ is the maximum angle of incidence for the SCML with a 0.80 mm thick substrate. For all meta-lenses depicted, $f = 1.0$ mm, $r = 1.0$ mm, $n_{sub} = 1.46$, and $n_m = 1$. For the meta-lenses in (a)–(e), substrate thickness $d = 0.50$ mm.

the HML is independent of the substrate thickness. Here, a meta-lens with no substrate is considered a theoretical limit of the finite-substrate-thickness case in the limit where the thickness goes to 0. At the maximum angle of incidence when TIR occurs, the magnitude of coma for the marginal rays at the edge of the HML is equal to the radius of the HML [ray diagram; Fig. 4(a)].

Figure 5(f) shows coma for the SCML. For the SCML, the maximum coma is smaller than the radius of the SCML due to the TIR limitation at the front surface of the substrate [ray diagram; Fig. 4(c)]. For larger substrates, this effect occurs at smaller angles of incidence and therefore leads to smaller coma. Figures 5(g) and 5(h) show, respectively, the difference in coma between the HML and SCML at two different angles of incidence. The SCML has less coma than the HML when the radial coordinate is small. As the radial coordinate increases, this behavior is reversed. This effect is even larger when the substrate thickness is increased.

Figures 6(a)–6(d) show the ray diagrams for Petzval field curvature and distortion of the HML and SCML with different
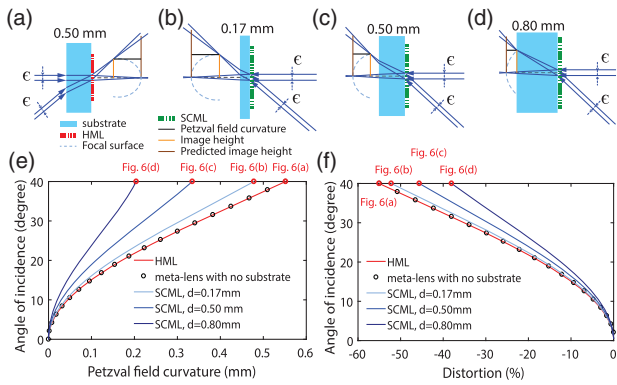
Fig. 6. Petzval field curvature and distortion of a HML and a SCML. (a)–(d) Ray diagrams of two chief rays for the HML and SCML with different substrate thicknesses d. When ϵ is very small, the intersection of those two chief rays defines the curved focal "plane", which deviates from the flat vertical plane (blue dashed line). (e) Petzval field curvature of the meta-lenses depicted in (a)–(d). Petzval field curvature for a certain angle of incidence is defined as the focal length shift parallel to the optical axis. Reference is normal incidence. The red dots indicate the corresponding ray diagram. (f) Distortion of the same meta-lenses. Distortion is defined as the relative difference between the actual image height and the predicted image height [Eq. (14)]. The predicted image height is the linear extrapolation of the image height at the center with γ_0 as a proportionality constant. For all meta-lenses depicted, $f = 1$ mm, $r = 1$ mm, $n_{sub} = 1.46$, $n_m = 1$. For the meta-lenses in (a)–(d), angles of incidence are $\theta = 0°$ and $\theta = 40°$.

substrate thicknesses. Petzval field curvature and distortion are defined by the focusing position of an oblique incident chief ray. The focusing position is defined as the intersection of two chief rays crossing the meta-lens plane at positions $\pm \epsilon$.

Petzval field curvature is the distance along the optical axis between the focusing position and the flat vertical plane as ϵ approaches 0 [36]. Imaging sensors like CMOS and CDD are flat; therefore, the focal point before the flat vertical plane causes an aberrated focal spot on the imaging sensor. Intuitively, distortion is the change in magnification across an image [36]. It is defined as the relative difference between the actual image height and the predicted image height:

$$\text{Distortion}(\%) = \left(\frac{h_a - h_p}{h_a} \right) \cdot 100. \tag{14}$$

Here h_a is the actual image height and h_p is the predicted image height. The actual image height, h_a, is the height of the focusing position of the two chief rays. For a given angle of incidence θ, the predicted image height is the extrapolated image height from the image center: $h_p = \gamma_0 \tan(\theta)$, with

$$\gamma_0 = f - d \left(\frac{n_{sub} - n_m}{n_m} \right). \tag{15}$$

For an imaging system with a working distance of d_f, γ_0 is related to the image center magnification M_0 as follows: $M_0 = \gamma_0 / d_f$. For most applications, distortion is not a limitation as it can be corrected with post-processing techniques. Figures 6(e) and 6(f) show, respectively, that the Petzval field curvature and distortion are smaller for the SCML than they are

for the HML. A larger substrate thickness decreases both Petzval field curvature and distortion. At an angle of incidence of 40°, the Petzval field curvature of the SCML with a substrate of 0.80 mm thickness is almost three times smaller compared with that of the HML. The HML and the meta-lens with no substrate are equivalent in terms of Petzval field curvature and distortion as smaller angles in the substrate of the HML are compensated for by a larger refractive index of the substrate—just as previously with coma.

7. CONCLUSION

To conclude, the SCML exhibits certain advantages over the HML. The higher NA of the SCML enables a smaller diffraction limit in a more compact configuration; in addition, monochromatic aberrations like Petzval field curvature and distortion are reduced. The higher NA of the SCML comes at the cost of a smaller maximum angle of incidence. In microscopy, the meta-lens nanostructures are better protected from outside world contaminants like dust and humidity in the SCML configuration, because of the small proximity to the specimen. In immersion microscopy, the SCML would allow designing the meta-lens in air and not in a liquid [37]. With dielectric meta-surfaces, this is easier because of the larger index contrast. More generally, our work provides an intuitive platform toward designing a meta-lens stacking, similar to the approach that has been developed by lens makers for bulky optical components, to systematically reduce aberrations and thus give a new impulse to applications of meta-lenses in the industry [38].

REFERENCES

1. N. Yu, P. Genevet, M. A. Kats, F. Aieta, J. P. Tetienne, F. Capasso, and Z. Gaburro, "Light propagation with phase discontinuities: generalized laws of reflection and refraction," Science **334**, 333–337 (2011).
2. N. Yu and F. Capasso, "Flat optics with designer metasurfaces," Nat. Mater. **13**, 139–150 (2014).
3. J. P. B. Mueller, N. A. Rubin, R. C. Devlin, B. Groever, and F. Capasso, "Metasurface polarization optics: independent phase control of arbitrary orthogonal states of polarization," Phys. Rev. Lett. **118**, 113901 (2017).
4. Y. W. Huang, W. T. Chen, W. Y. Tsai, P. C. Wu, C. M. Wang, G. Sun, and D. P. Tsai, "Aluminum plasmonic multicolor meta-hologram," Nano Lett. **15**, 3122–3127 (2015).
5. H. N. S. Krishnamoorthy, Z. Jacob, E. Narimanov, I. Kretzschmar, and V. M. Menon, "Topological transitions in metamaterials," Science **336**, 205–209 (2012).
6. Y. Z. Liu, J. W. Dong, Y. Y. Pu, B. Chen, H. X. He, and H. Wang, "High-speed full analytical holographic computations for true-life scenes," Opt. Express **18**, 3345–3351 (2010).
7. M. Khorasaninejad, W. T. Chen, R. C. Devlin, J. Oh, A. Zhu, and F. Capasso, "Meta-lenses at visible wavelengths: diffraction-limited focusing and sub-wavelength resolution imaging," Science **352**, 1190–1194 (2016).
8. S. A. Bedini, "Lens making for scientific instrumentation in the seventeenth century," Appl. Opt. **5**, 687–694 (1996).

9. T. Stone and N. George, "Hybrid diffractive-refractive lenses and achromats," Appl. Opt. **27**, 2960–2971 (1988).

10. D. Faklis and G. M. Morris, "Spectral properties of multiorder diffractive lenses," Appl. Opt. **34**, 2462–2468 (1995).

11. D. W. Sweeney and G. E. Sommargren, "Harmonic diffractive lenses," Appl. Opt. **34**, 2469–2475 (1995).

12. F. Aieta, M. A. Kats, P. Genevet, and F. Capasso, "Multiwavelength achromatic metasurfaces by dispersive phase compensation," Science **347**, 1342–1345 (2015).

13. M. Khorasaninejad, Z. Shi, A. Zhu, W. T. Chen, V. Sanjeev, and F. Capasso, "Achromatic meta-lens over 60 nm bandwidth in the visible and metalens with reverse chromatic dispersion," Nano Lett. **17**, 1819–1824 (2017).

14. S. Wang, P. C. Wu, V. Su, Y.-C. Lai, C. Hung Chu, J.-W. Chen, S.-H. Lu, J. Chen, B. Xu, C.-H. Kuan, T. Li, S. Zhu, and D. P. Tsai, "Broadband achromatic optical metasurface devices," Nat. Commun. **8**, 187 (2017).

15. Y. Soskind, _Field Guide to Diffractive Optics_ (SPIE, 2011).

16. G. J. Swanson, "Binary optics technology: the theory and design of multi-level diffractive optical elements," Technical Report 854, DTIC Document (Lincoln Laboratory, 1989).

17. M. B. Stern, "Binary optics: a VLSI-based microoptics technology," Microelectron. Eng. **32**, 369–388 (1996).

18. M. Khorasaninejad, F. Aieta, P. Kanhaiya, M. A. Kats, P. Genevet, D. Rousso, and F. Capasso, "Achromatic metasurface lens at telecommunication wavelengths," Nano Lett. **15**, 5358–5362 (2015).

19. M. Khorasaninejad, W. T. Chen, J. Oh, and F. Capasso, "Super-dispersive off-axis meta-lenses for compact high resolution spectroscopy," Nano Lett. **16**, 3732–3737 (2016).

20. A. Arbabi, Y. Horie, A. J. Ball, M. Bagheri, and A. Faraon, "Subwavelength-thick lenses with high numerical apertures and large efficiency based on high-contrast transmitarrays," arXiv:1410.8261 (2014).

21. K. Esswein, "Attachment of microscope objectives," U.S. patent 4,515,439 (07 May 1985).

22. M. Abramowitz, K. R. Spring, H. E. Keller, and M. W. Davidson, "Basic principles of microscope objectives," BioTechniques **33**, 772–781 (2002).

23. T. Ito and S. Okazaki, "Pushing the limits of lithography," Nature **406**, 1027–1031 (2000).

24. F. Aieta, P. Genevet, M. A. Kats, N. Yu, R. Blanchard, Z. Gaburro, and F. Capasso, "Aberration-free ultrathin flat lenses and axicons at telecom wavelengths based on plasmonic metasurfaces," Nano Lett. **12**, 4932–4936 (2012).

25. F. Aieta, P. Genevet, M. Kats, and F. Capasso, "Aberrations of flat lenses and aplanatic metasurfaces," Opt. Express **21**, 31530–31539 (2013).

26. B. Groever, W. T. Chen, and F. Capasso, "Meta-lens doublet in the visible," Nano Lett. **17**, 4902–4907 (2017).

27. A. Arbabi, E. Arbabi, S. M. Kamali, Y. Horie, S. Han, and A. Faraon, "Miniature optical planar camera based on a wide-angle metasurface doublet corrected for monochromatic aberrations," Nat. Commun. **7**, 13682 (2016).

28. F. Bociort, "Optical system optimization," in _Encyclopedia of Optical Engineering_ (2003), Vol. **2**, pp. 1843–1850.

29. M. Peschka, F. Blechinger, H. Gross, and H. Zuegge, _Handbook of Optical Systems: Vol. 3. Aberration Theory and Correction of Optical Systems_ (Wiley, 2007).

30. A. She, S. Zhang, S. Shian, D. R. Clarke, and F. Capasso, "Large area electrically tunable lenses based on metasurfaces and dielectric elastomer actuators," arXiv:1708.01972 (2017).

31. B. Groever, "Matlab code for virtual focal length," (2017) [Retrieved 23 October 2017]; https://doi.org/10.6084/m9.figshare.5527954.

32. S. Sun, Q. He, S. Xiao, Q. Xu, X. Li, and L. Zhou, "Gradient-index meta-surfaces as a bridge linking propagating waves and surface waves," Nat. Mater. **11**, 426–431 (2012).

33. S. Sun, K.-Y. Yang, C.-M. Wang, T.-K. Juan, W. T. Chen, C. Y. Liao, Q. He, S. Xiao, W.-T. Kung, G.-Y. Guo, L. Zhou, and D. P. Tsai, "High-efficiency broadband anomalous reflection by gradient meta-surfaces," Nano Lett. **12**, 6223–6229 (2012).

34. B. C. Kress and P. Meyrueis, _Applied Digital Optics: From Micro-optics to Nanophotonics_ (Wiley, 2009).

35. Z. Lin, B. Groever, F. Capasso, A. W. Rodriguez, and M. Loncar, "Topology optimized multi-layered meta-optics," arXiv:1706.06715 (2017).

36. W. J. Smith, _Modern Optical Engineering_ (Tata McGraw-Hill Education, 1966).

37. W. T. Chen, A. Y. Zhu, M. Khorasaninejad, Z. Shi, V. Sanjeev, and F. Capasso, "Immersion meta-lenses at visible wavelengths for nanoscale imaging," Nano Lett. **17**, 3188–3194 (2017).

38. R. Kingslake, _A History of the Photographic Lens_ (Elsevier, 1989).